Journal of Power Sources 233 (2013) 166–173

Contents lists available at SciVerse ScienceDirect

Journal of Power Sources

journal homepage: www.elsevier.com/locate/jpowsour

Electrochemical lithiation and delithiation performance of SnSb–Ag/carbon nanonube composites for lithium-ion batteries

Peixin Zhang [a,*], Yanyi Wang [a], Yang Wang [a], Xiangzhong Ren [a], Kun Liu [b], Shiguo Chen [c,**]

[a] School of Chemistry and Chemical Engineering, Shenzhen University, Shenzhen 518060, PR China
[b] School of Chemistry and Chemical Engineering, Guangxi University, Nanning 530004, PR China
[c] School of Materials Science and Engineering, Shenzhen University, Shenzhen 518060, PR China

HIGHLIGHTS

- The coexistence of Ag and CNTs has synergetic effect on electrochemical properties.
- The ambient temperature affect the electrochemical properties.
- The CV curves and voltage profiles shows the cycle processes.
- The SEM micrographs show the relationship between structure and performance.

ARTICLE INFO

Article history:
Received 9 April 2012
Received in revised form
3 December 2012
Accepted 17 January 2013
Available online 1 February 2013

Keywords:
Alloy
Anode material
Electrochemical performance
Carbon nanonube

ABSTRACT

SnSb–Ag/Carbon nanonube (CNT) composites materials are synthesised using chemical reduction methods. The microstructure, morphologies and electrochemical properties of these materials are investigated by X-ray diffraction (XRD), field-emission scanning electron microscopy (FE-SEM), constant current charge/discharge tests and cyclic voltammetry tests. The results indicate that Ag promotes the entire charge–discharge process during the complex multi-step reaction process and, to some extent, prevent the reunion of nanoparticles. At the same time, CNTs, with a large space volume and form a network structure, prevent particles aggregation and increase the buffer space between the alloy particles, which greatly reduce the diffusion distance of lithium ions and the occurrence of lithium trapping in the active electrode materials. CNTs also have excellent mechanical properties and toughness, they effectively buffer enormous stresses during the volume expansion of alloy particles, weakening the forces between the particles and reducing the rate of formation of powder particles. All these factors cause the $SnSbAg_{0.1}$/6% CNT composites exhibit excellent cycle life by controlling the lithiation of the anode material; the reversible capacity for the 50th cycle is 639.6 mAh g^{-1} between 0.05 and 1.5 V.

1. Introduction

In recent years, a variety of portable electronic devices and electric vehicles have been rapidly developed and widely applied, which has created an urgent demand for high-energy lithium-ion batteries with long cycle life. The anode material plays a decisive role in a high-energy lithium-ion battery. Graphites and modified graphites have been widely used as anode materials in commercial lithium-ion batteries; however, because of the intrinsic limitations of these materials, the batteries cannot match the performance of high-energy lithium-ion batteries. Tin (Sn) has attracted widespread attention because it has a high specific capacity and an appropriate intercalation potential [1–3]. However, the Sn anodes undergo severe structural and volume changes during the lithiation/delithiation process, which result in poor cycle stability and seriously affect their use in industrial applications. The formation of alloys of Sn with active or inert metals can effectively alleviate the volume expansion and improve the cycling performance. Examples of representative Sn-based alloys used for this purpose include SnSb, Cu_6Sn_5 and NiSn [4–7]. Among these Sn-based alloys, the SnSb intermetallic compound and its derivatives have attracted particular attention because both Sn and Sb have the capacity to store lithium, which results in a higher theoretical specific capacity than other active/inert systems, such as SnCu and SnNi. Another

* Corresponding author. Tel./fax: +86 755 26558134.
** Corresponding author. Tel./fax: +86 755 26534457.
E-mail addresses: pxzhang@szu.edu.cn, pxzhang96@yahoo.com (P. Zhang), csg@szu.edu.cn (S. Chen).

0378-7753/$ – see front matter © 2013 Elsevier B.V. All rights reserved.
http://dx.doi.org/10.1016/j.jpowsour.2013.01.097

advantage of the SnSb compound is that stepwise lithiation processes can relieve volume changes [8–10].

Many studies have confirmed that reducing the active particle size to the nanometer range (<100 nm) in alloy anodes can significantly improve their performance during cycling. As the grain size decreases to the nanometer scale, the motion and pile-ups of dislocations (responsible for premature cracking and fracturing of anodes) are limited or prevented [11,12]. This result implies that nanocomposite anodes can sustain much higher stresses than other anodes before they are pulverised. In our previous work, SnSb–Ag nano-alloy anode materials were prepared by a chemical reduction method; these materials had a relatively high specific capacity (518 mAh g^{-1} after 50 cycles) and good cycle performance [13]. However, nano-particles also have some shortcomings, such as large surface areas, long diffusion distances and facile agglomeration, which hinder their use in industrial applications.

An effective approach to overcome this problem is to load the nanoparticles onto carbon-based matrices, such as carbon [14], amorphous carbon [15], mesophase carbon microbeads [16] and hard carbon spherules [17]. Compared with the other carbon materials mentioned above, the carbon nanotubes are more attractive due to their unique electronic properties and their mechanical properties, such as stiffness, strength, and resilience, which exceed those of all other materials currently in use [18,19]. Recent research has demonstrated that the electrochemical performance of some Sn-based metals, oxides and alloys can be significantly improved using CNTs (carbon nanotubes) as additives or compounds [20–22]. The flexible CNTs not only accommodate the volume changes and suppress the aggregation of the nanoparticles but also provide conductive channels and contribute to the overall capacity of the anodes [23]. Park et al. [21] studied nano-sized SnSb/MWNT composite materials prepared by a chemical reduction process, and Jhan et al. [24] studied Sn–C/C(MWNT) composite materials prepared by a carbothermal reduction method; in both studies, the cycle performance was excellent. However, due to the large volume effect of Sn and SnSb materials, Park et al. and Jhan et al. added high concentrations of CNTs, 52.4 and 63.9 wt.%, respectively, which greatly reduced the capacity of these alloyed anode materials.

In this work, we attempted to synthesise SnSb–Ag/CNT composite alloy anode materials to further improve the cycle performance and reduce the raw material costs. The electrochemical performance of SnSb–Ag/CNT composite anodes was studied by controlling the content of Ag and CNTs and the cut-off voltage. The dependence of the cyclic behaviour of the composite anode electrodes and their microstructure is discussed. The underlying mechanism for the improvement in electrochemical properties was investigated by electrochemical impedance spectroscopy.

2. Experimental

To produce the SnSb–Ag/CNT composite powders, the unprocessed CNTs (diameter approximately 60–100 nm, length 15 μm) were added to 65% (v/v) concentrated HNO_3, refluxed at 120 °C for 5 h, filtered, washed and dried. The pre-process CNTs were dispersed in 0.2 M aqueous $NaBH_4$ solution (pH > 12) by ultrasound for 40 min. Excess $NaBH_4$ was used to ensure the complete reduction of the metal ions. A 0.1 M aqueous solution of $SbCl_3$, $SnCl_2$ and $C_6H_5Na_3O_7$ with the molar ratio of 1:1:3.5 and a 0.1 M aqueous solution of $AgNO_3$ were prepared. All reagents were of analytical grade. The reduction was performed by adding the $AgNO_3$ solution drop wise to the $NaBH_4$/CNT solution and then by adding the $SbCl_3$/$SnCl_2$ solution with vigorous magnetic stirring at room temperature. After the reaction, the mixture was dispersed ultrasonically for 2 h and then aged in a water bath maintained at 80 °C for 3 h. The product was filtered, washed with deionised water and acetone, and dried at 105 °C for 10 h under a vacuum. The composite powder was ground in an agate mortar, sifted with 100 mesh sieve and stored in a glove box under an Ar atmosphere.

Phase identification for the alloy powders was performed with a D8ADVANCE X-ray diffraction (XRD) instrument. The microstructure and morphology of the particles was determined using field-emission scanning electron microscopy (FE-SEM) on Hitachi SU-70 instruments.

The typical electrodes were prepared by mixing 90 wt.% active materials, 7 wt.% acetylene black and 3 wt.% polyvinylidene fluoride (PVDF) dissolved in N-methylpyrrolidone (NMP). Electrochemical studies of the synthesised materials were performed with coin cells that were assembled in an Ar-filled glove box. Each coin cell consisted of a metallic lithium foil as a counter electrode, 1 M $LiPF_6$ in ethylene carbonate (EC) and dimethyl carbonate (DMC) (1:1 v/v) as an electrolyte, Celegard 2400 as a separator and the synthesised composite alloy as a working electrode. A CT2001A battery tester was used to perform cycling tests between 0.1 and 1.5 V with a constant current density of 0.15 mA cm^{-2} at a constant temperature of 25 °C, unless otherwise noted. Cyclic voltammetry tests were performed using a Solartron 1470e electrochemical testing system in the range between 0 and 2.0 V (vs. Li/Li^+) at a scan rate of 0.05 mV s^{-1}.

3. Results and discussion

3.1. Phase structures and morphologies

Fig. 1 shows the XRD patterns of $SnSbAg_{0.1}$ and $SnSbAg_{0.1}$/6% CNT composite materials obtained by the chemical reduction method. Based on these data, the diffraction pattern of the composite contains sharp SbSn peaks and weak $Ag_{3-4}Sn$ and Sn peaks. The SnSb is a non-stoichiometric compound and consists chiefly of a rhombohedral structure in the β-SnSb phase where the atomic ratio of Sb to Sn exceeds 1; according to research, SnSb contains 59.7 at% Sb [25]. If the reaction is carried out with a 1:1 ratio of Sb:Sn, the excess Sn (which is not incorporated in the alloy) will form pure Sn crystals. The peaks for Ag were weak because the dissolved Ag reacted with the surplus Sn to form $Ag_{3-4}Sn$ under the reaction conditions (in an 80 °C water bath), and there was a low concentration of Ag. The $SnSbAg_{0.1}$/CNT composite materials contained only low levels of CNTs, and the CNT peak was weak compared with the SbSn peak. The CNT peaks are mostly invisible in the XRD patterns of $SnSbAg_{0.1}$/6% CNTs composite materials, and the

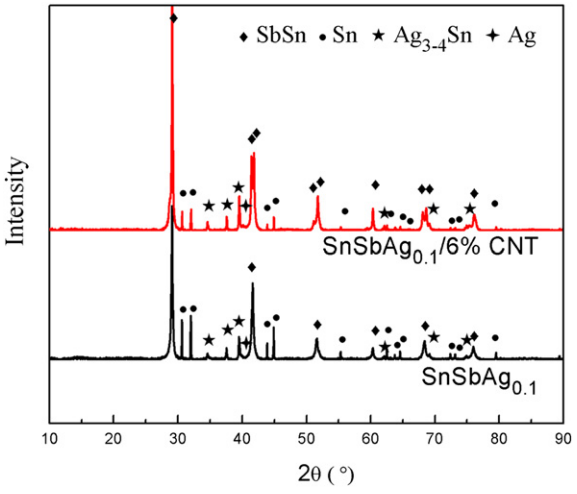

Fig. 1. XRD patterns of (a) $SnSbAg_{0.1}$ and (b) $SnSbAg_{0.1}$/6% CNT composite materials.

XRD patterns of $SnSbAg_{0.1}$/6% CNT composite materials are essentially the same as the patterns for $SnSbAg_{0.1}$.

Fig. 2 shows the FE-SEM images of the $SnSbAg_{0.1}$ and the $SnSbAg_{0.1}$/6% CNT composite materials at different magnifications. From Fig. 2a and b, it is apparent that the nanoparticles do not vary greatly but aggregate significantly due to their relatively large specific surface area and surface energy. In Fig. 2c and d, all the CNTs are approximately 60–100 nm in diameter and unbroken, and the nano-sized $SnSbAg_{0.1}$ composite materials are captured in the CNTs network. During the process of chemical reduction, the CNTs (which are approximately 15 μm long) distribute themselves evenly throughout the solution under ultrasonic mixing and entangled. This behaviour lays the foundation for a homogeneous dispersion of alloy particles in the network structure of CNTs and greatly reduces the aggregation of the nanoparticles and increases the spaces between particles.

3.2. The electrochemical properties of the SnSb–Ag/CNT composite materials

3.2.1. The cycling properties of the $SnSbAg_{0.1}/x$ CNT composite materials

Fig. 3 compares the cycling properties of $SnSbAg_{0.1}/x$ CNT ($x = 0$, 4, 6, 8 and 10 wt.%) composite anode materials between 0.1 and 1.5 V at room temperature. The results indicate that the first discharge capacity of the $SnSbAg_{0.1}/x$ CNT composites (x = 0, 4, 6, 8 and 10 wt.%) are 1083.7, 955.2, 953.3, 966.8 and 944.4 mAh g^{-1}, respectively; these values far exceed the theoretical capacity. During the syntheses, tin and antimony oxides were inevitably generated and likely reacted with the lithium, thereby artificially enhancing the first capacities. The reaction of metal oxide compounds with lithium is irreversible, and the first irreversible capacity is greatly increased. The $SnSbAg_{0.1}$ alloy anodes show the highest first discharge capacity, but the capacity rapidly decreases, the discharge capacity is 402.9 mAh g^{-1} after 50 cycles, which is far lower than the capacity of $SnSbAg_{0.1}/x$ CNT in the subsequent cycles. With the addition of CNTs, the electrochemical performance of the $SnSbAg_{0.1}/x$ CNT compounds improves significantly. When the CNT content is 4%, the composite discharge capacity is 488.2 mAh g^{-1} after 50 cycles, and there are improvements in the cycling performance, although the capacity decreases relatively rapidly. When the CNT content is over 6%, the composites exhibit good cycle stability and high capacity. In Fig. 3, the relative reduction of the first irreversible capacity with the addition of CNTs is apparent. The results indicate that the first irreversible capacity of $SnSbAg_{0.1}/x$ CNT (x = 0, 4, 6, 8 and 10 mass%) composites are 406.8, 233.3, 223.2, 241.4 and 205.8 mAh g^{-1}, respectively. Due to the intricate network structure of the large-diameter CNTs, the aggregates of the nanoparticles are smaller, and the spaces between particles are larger, which is beneficial to the deintercalation of lithium and reduced the capture of lithium by the alloy particles.

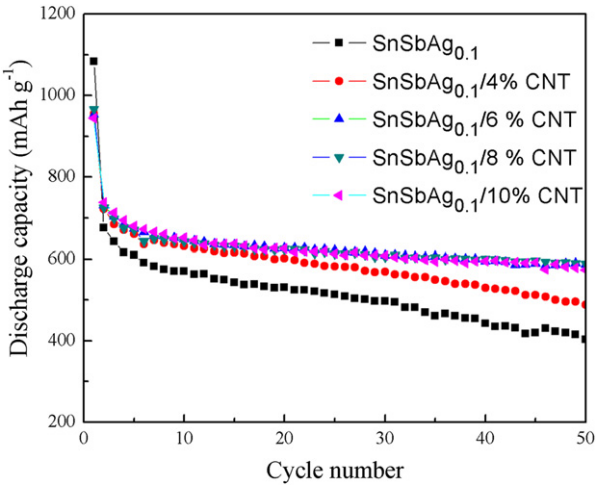

Fig. 3. Cycling performance of $SnSbAg_{0.1}/x$ CNT composite materials.

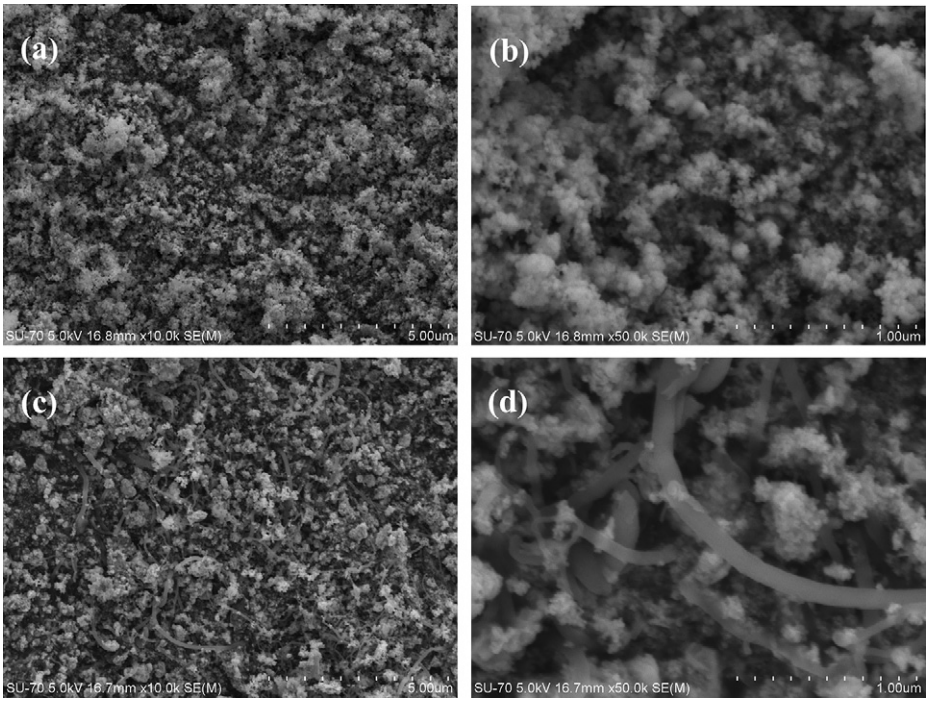

Fig. 2. FE-SEM images of (a, b) $SnSbAg_{0.1}$ composites and (c, d) $SnSbAg_{0.1}$/6%CNT composites at different magnifications.

3.2.2. The cycling properties of $SnSbAg_x$/6% CNT composite materials

In recent years, SnSb/CNT composite materials have been extensively studied, and most of composite materials contained high levels of CNTs and displayed good cycling performance. However, a few researchers obtained good results when they used low levels of CNTs. Silver plays an important role in the $SnSbAg_{0.1}$/CNT composite materials. Fig. 4 shows a comparison of the cycling performance of SnSb/6% CNT, $SnSbAg_{0.1}$/6% CNT and $SnSbAg_{0.2}$/6% CNT compounds. The first discharge capacity of SnSb/6% CNT composite is 1046.3 mAh g^{-1}; the charge capacity gradually decreased in the subsequent cycles, and discharge capacity was 491.4 mAh g^{-1} after 50 cycles. The first discharge capacities of $SnSbAg_{0.1}$/6% CNT and $SnSbAg_{0.2}$/6% CNT composites are 953.3 and 933.5 mAh g^{-1}, respectively, and the discharge capacities are 586.1 and 567.4 mAh g^{-1} after 50 cycles, respectively, to maintain a relatively stable trend after the second cycle. The reason for this behaviour is that the presence of Ag reduces the degree of alloying and changes the parent phases; the Li extraction–insertion process occurs in multiple steps and increases the cycling performance of the composite materials. At the same time, the capacity of Ag is lower than Sn and Sb, increasing the Ag content decreases the overall capacity of a composite.

3.2.3. The cycling properties of $SnSbAg_{0.1}$/6% CNT composite anode materials at different temperatures

Studies showed that the ambient temperature has an effect on the electrochemical cycling properties of composite alloy anode materials. Fig. 5 compares the cycling performance of $SnSbAg_{0.1}$/6% CNT nanocomposite materials at −25 °C, 0 °C, 25 °C and 55 °C. The composite alloy anode materials show very smooth cycling performance at 0 °C and −25 °C; their capacity loss rates are approximately 1.94% and 2.57% per cycle between 2 and 50 cycles, respectively (although the initial and retained capacities are very low). At 0 °C and −25 °C, their initial capacities are 696.25 and 723.00 mAh g^{-1}, and their retained capacities are 500 and 528 mAh g^{-1}, respectively. At 25 °C and 55 °C, the initial capacity of the $SnSbAg_{0.1}$/6% CNT electrodes are 953.30 and 988.24 mAh g^{-1}, respectively, which obviously are larger than the electrodes at lower environmental temperatures. Although they showed relatively rapid capacity fading in the subsequent cycles (3.95%, and 4.12% loss/cycle), the retained capacities (586.1 and 612.7 mAh g^{-1} after 50 cycles) are still higher than that at the lower temperatures. At high temperatures, the interfacial impedance and the polarisation of the electrodes decrease, the rate of movement of the lithium ions accelerates, the lithium ions are easy to intercalate and extract from the electrode and the capacity is relatively higher. However, these changes expand the nano-particle volumes, cause relatively serious damage to the particles and the electrode in the course of swelling and lead to relatively poor cycling properties. At low temperatures, the interfacial impedance and electrolyte viscosity increase, the diffusion resistance increases and the diffusion rate of the lithium ions decreases. These changes are accompanied by significant electrode polarisation, reduction in the discharge voltage plateau and the capacity, insufficient lithium intercalation and smaller expansion of the volume, which effectively prevent the particles from becoming powders during the cycles and greatly improve the cycling properties of the composite alloy anode materials.

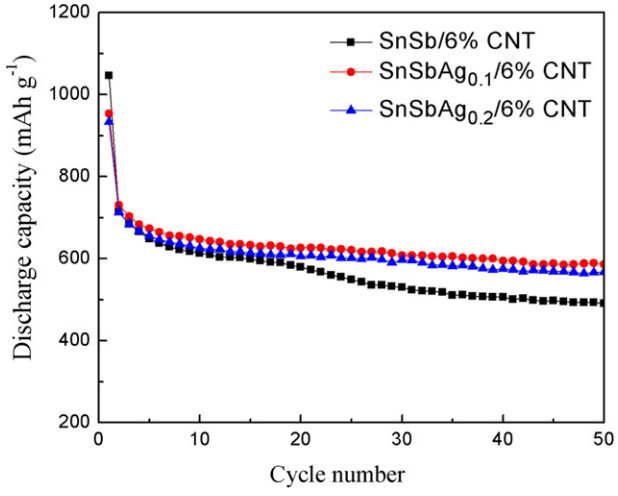

Fig. 4. Cycling performance of SnSb–Ag_x/6% CNT composite materials.

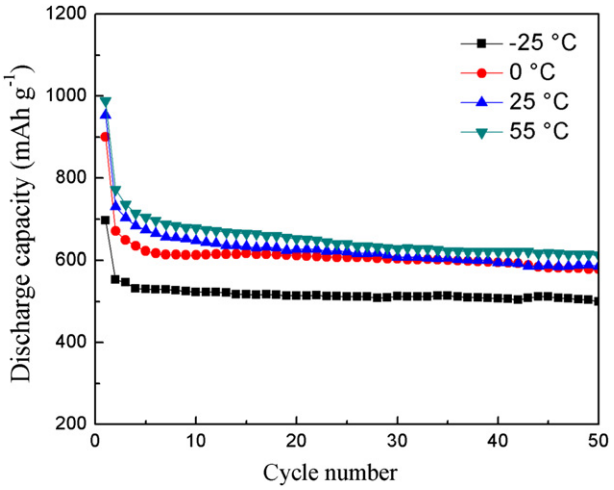

Fig. 5. Cycling performance of $SnSbAg_{0.1}$/6% CNT composite materials at different temperatures.

3.2.4. Cycling performance of $SnSbAg_{0.1}$/6% CNT nanocomposite materials in different voltage regions

Research indicate [26,27] that the cycle life of alloy anodes is much better cycle life when the anodes are cycled within a limited voltage range rather than the full voltage range. The cycling stability can be improved by restricting either the upper or lower cutoff voltage, which reduces the amount of volume change, the tendency for particle aggregation and the extent of structural changes that take place during cycling. In previous work, the authors observed that SnSb–Ag composites showed better cycle performance when they controlled the lithiation degree of Ag by restricting the charge and discharge voltage between 0.1 and 1.5 V [13]. With the addition of the CNTs, the mechanism improved and regained control of the voltage ranges for better cycling performance and higher capacity. Fig. 6 shows the cycling performance of SnSbAg0.1/6% CNT nanocomposite materials in different voltage regions. When the cut-off voltage is 0.02 V, the initial discharge capacity and initial irreversible capacity are 1040.3 and 258.5 mAh g^{-1}, respectively. The specific capacity begins to decrease as the charging and discharging cycles progress. The Li adequately reacts with the alloy particles when discharged to 0.02 V, which intensifies the volume expansion of the alloy particles, causes the lithium ion extractions to be more difficult and somewhat increases the initial irreversible capacity. The complete reaction between Ag and Li, caused by the rupture of the Ag particles, and the loss of contact between the particles and the copper foil occur easily, hindering the positive role played by Ag in the process of lithium deintercalation and affecting the cycling

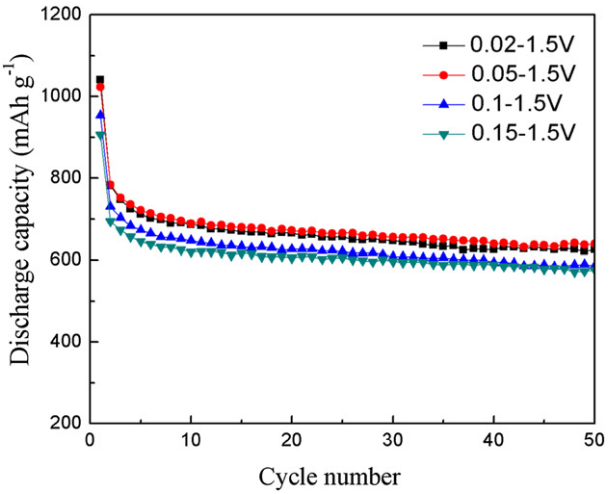

Fig. 6. Cycling performance of $SnSbAg_{0.1}$/6% CNT composite materials in different voltage regions.

stability. When the lower cutoff voltage is 0.05 V, $SnSbAg_{0.1}$/6% CNT exhibits excellent cycling performance. Under these conditions, the first discharge capacity (943.5 mAh g^{-1}) is slightly lower than during discharge to 0.02 V; however, the initial irreversible capacity (241.9 mAh g^{-1}) is lower, and the discharge capacity is higher than during discharge to 0.02 V in subsequent cycles. The electrode maintains a rechargeable capacity as high as 639.6 mAh g^{-1} after 50 cycles, which is much higher than the Ag–Sb–Sn nanocomposite anode obtained by mechanical alloying techniques and the SnSb–Ag nanocomposite anode obtained by a co-reduction method [13,28]. However, after 50 cycles, the retained capacities for discharge to 0.1 and 0.15 V (586.1 and 576.3 mAh g^{-1}, respectively) are lower than for discharge to 0.05 V. The cycling stability is equivalent to that for discharge to 0.05 V.

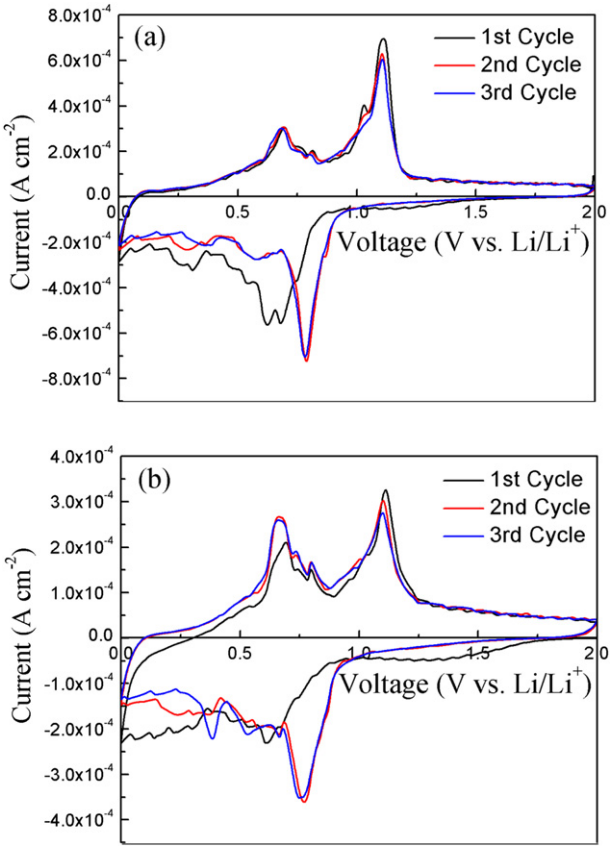

Fig. 7. CV for (a) $SnSbAg_{0.1}$ and (b) $SnSbAg_{0.1}$/6% CNT composite materials.

3.3. Relationship between structural changes and cycling performance

Fig. 7 shows the cyclic voltammetry curves for $SnSbAg_{0.1}$ and $SnSbAg_{0.1}$/6% CNT composite materials. The $SnSbAg_{0.1}$/6% CNT contains only a low concentration of CNTs; the cyclic voltammetry curves for $SnSbAg_{0.1}$/6% CNT are very similar to those for $SnSbAg_{0.1}$. For the cathodic scan, a weak reduction peak was present in the first

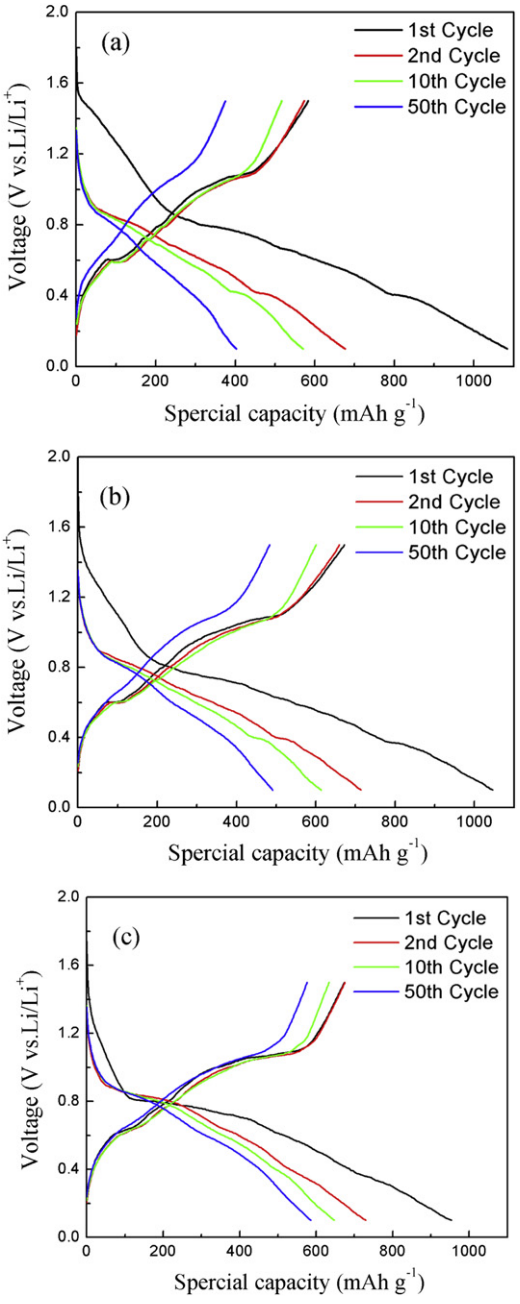

Fig. 8. The discharge and charge profiles of (a) $SnSbAg_{0.1}$; (b) SnSb/6% CNT; and (c) $SnSbAg_{0.1}$/6% CNT electrodes for the 1st, 2nd, 10th and 50th cycle.

cycle at 1.5–0.8 V, but this peak did not appear in subsequent cycles, indicating that there were one or more irreversible reduction reactions. According to the literature, Sb_2O_3 and SnO have similar reduction peaks at 1.5–0.8 V for the Li insertion process. Based on this Li insertion alloying mechanism, the following reduction reaction is proposed: $xLi^+ + e^- + (Sb_2O_3;SnO)_{surface} \rightarrow Li_2O + (Sb, Sn)_{surface}$ [25]. In addition, the decomposition of the electrolyte occurred under 1.2 V; this interval contains the decomposition of the electrolyte and the formation of SEI films [17]. When the voltage is 0.8 V, a strong double reduction peak is observed in the first cycle, but the single peak appears in subsequent cycles, indicating that the process contains one reversible and one irreversible reduction reaction. The formation of SEI films at 1.2–0.2 V, the irreversible reaction in this interval, is the decomposition of the electrolyte [17]. Jin et al. [28] tested the structural change of $Ag_{36.4}Sb_{15.6}Sn_{48}$ during electrode charge and discharge in a different voltage range by XRD and found that the SnSb peak completely disappeared, the Li_3Sb peak appeared and the Sn peak was enhanced between 0.83 and 0.66 V. This process also corresponds to the reversible reaction of the SnSb and Li: $SnSb + Li + 3e \rightarrow Li_3Sb + Sn$. A series of peaks are observed that correspond to Li insertion reactions with both the native and extruded Sn and $Ag_{3-4}Sn$ from 0.66 to 0 V; these reactions form a series of alloys: Li_xSn, $Ag_2LiSn/AgLi_2Sn$ and Li_xAg. In Fig. 7b, the intensity of the peak was significantly stronger than for the peaks in Fig. 7a between 0.25 and 0 V because this interval contains the Li insertion processes of CNTs. For the anodic scan, the peaks in Fig. 7a and b are similar and appear to resemble a series of the oxidation peaks that correspond to a series extraction reaction of Li. The CV curves of the two electrode materials coincide closely after subsequent cycles, which show that they have good cycling performance. In the curves of the first cycle and the subsequent cycles of $SnSbAg_{0.1}$/6% CNT composite alloy anode materials, the current appears to undergo a very small decrease, which shows that $SnSbAg_{0.1}$/6% CNT has a better cycling performance than $SnSbAg_{0.1}$.

Fig. 8 shows the voltage profiles of the $SnSbAg_{0.1}$, the SnSb/6% CNT and the $SnSbAg_{0.1}$/6% CNT electrodes for the 1st, 2nd, 10th and 50th cycle. The voltage profiles curve from the 1st cycle and the subsequent cycles are very different. For all three electrodes, there is a slope between 1.6 and 0.8 V due to the first discharge process, which corresponds to the reduction of alloy granule surface oxide compound. The slopes appear at 1.2 V after the subsequent cycles and correspond to the decomposition of the electrolyte and the formation of SEI films. These changes in the slopes were consistent with many observations that were reported in the literature [17]. Therefore, the slopes correspond to the reduction of the alloy granule surface oxide compound, the decomposition of the electrolyte and the formation of SEI films between 1.6 and 0.8 V. The irreversible capacity was biggest for $SnSbAg_{0.1}$, followed by SnSb/6% CNTs; the smallest was $SnSbAg_{0.1}$/6% CNTs. If the particles are less than 100 nm, the particles would agglomerate due to the overwhelming driving forces to reduce their surface energy [21]. In the process of the agglomeration of particles, oxidation films were observed to form on the surfaces when there was sufficient contact with oxygen. The addition of CNTs greatly reduces the surface energy of the composites. The network structure formed by the CNTs effectively prevented the agglomeration of the particles, reduced the particle motion and the contact time of the particles with air, decreased oxide formation and thereby reduced the irreversible capacity.

The potential plateau at approximately 0.8 V, corresponded to the alloying reaction of SnSb with lithium to form Li_3Sb and Sn. Lithium further reacts with Sn and $Ag_{3-4}Sn$ to form various compounds: Li_xSn, $Ag_2LiSn/AgLi_2Sn$ and Li_xAg [28]. It can be observed from the first discharge and charge curves that the initial irreversible capacity loss of these three materials mainly results from the Li insertion processes below 0.8 V. The high surface energy of the nano-alloy particles usually drives the agglomeration; it is difficult to disperse the aggregates once they are formed. During the aggregation process, the particles stick together tightly, and small metal particles combine to form larger particles. The SEI films that formed on the surface of nano-particles cannot prevent the agglomeration of the particles; these films promote agglomeration by connecting the particles. The SEI films destroy the electrical conductivity of the activity of the nano-alloy particles. When the nano-alloy particles with SEI films are inserted deeply in the aggregates, the particles lose contact with the current collector and other particles. At the same time, the agglomeration increases the lithium-ion diffusion distances, reduces the insertion point of the lithium and ultimately reduces the overall capacity.

The $SnSbAg_{0.1}$ anode material is only composed of the nanoparticles; as a result, significant aggregation occurs, and the first irreversible capacity is highest. However, the SnSb/6% CNT and SnSbAg0.1/6% CNT composites effectively prevent the agglomeration of the nano-alloy particles and thereby reduce the first irreversible capacity. The presence of Ag triggers the entire discharge in a complex multi-step reaction process and prevents the extruded Sn from aggregating to complete the reactions to reduce the first irreversible capacity of the $SnSbAg_{0.1}$/6% CNTs and enhance the electrochemical properties. In the subsequent multiple cycle process, the SnSb/6% CNT and $SnSbAg_{0.1}$/6% CNT anodes have good cycling stability because CNTs have strong mechanical compatibility and toughness, which enable them to maintain electronic conduction channel stability and effectively alleviate the volume expansion of alloy nanoparticles during the Li insertion and extraction processes. After several cycles, the $SnSbAg_{0.1}$ electrode underwent volume expansion, which caused the material to become a powder and fall off of the nano-particles; the results of

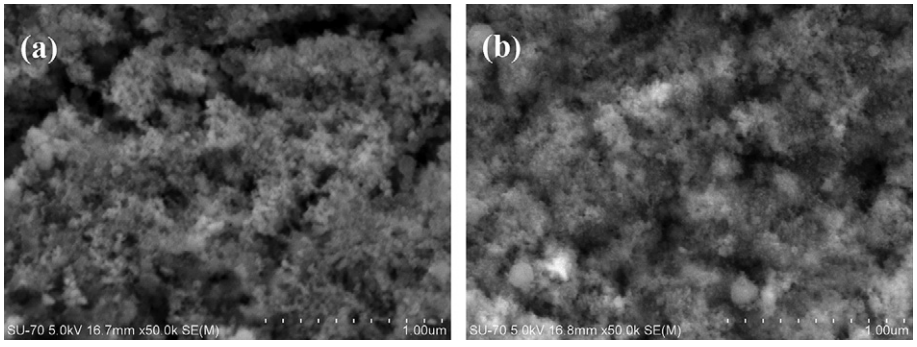

Fig. 9. FE-SEM images of $SnSbAg_{0.1}$ electrode: (a) before cycling; (b) after 10 cycles.

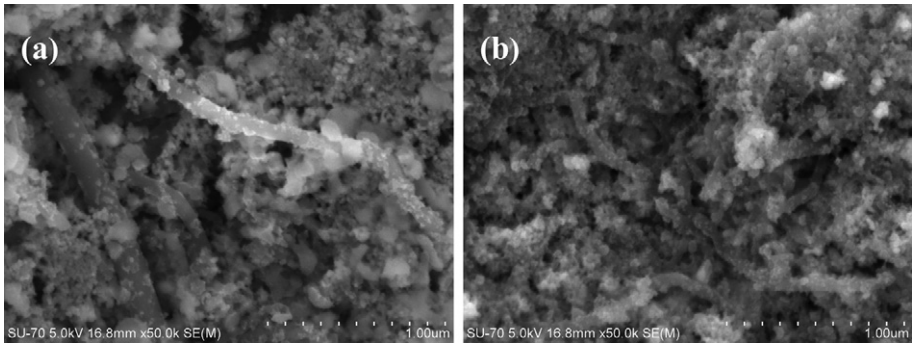

Fig. 10. FE-SEM images of $SnSbAg_{0.1}$/6% CNT electrode: (a) before cycling; (b) after 10 cycles.

this behaviour were reductions in the amount of active material on the electrodes and the specific capacity, which decreased the cycling performance.

Figs. 9 and 10 show SEM micrographs of the surface of $SnSbAg_{0.1}$ and $SnSbAg_{0.1}$/6% CNT composite electrodes before cycling and after 10 cycles. For the $SnSbAg_{0.1}$ alloy nano-particles, there is a significant amount of aggregation, and the distribution of the particles on the copper foil is disordered. In contrast, the particles and CNTs are evenly dispersed on the copper on the $SnSbAg_{0.1}$/6% CNT composite electrodes, and the particles are distributed uniformly in the CNT webs where they prevent agglomeration and bind the particles in their network before cycling is performed. After 10 cycles, the particle size in the $SnSbAg_{0.1}$ alloy electrode was smaller than before cycling. During the Li insertion process, the particles expand, and their buffer spaces are smaller; this behaviour alleviates the strain that can form bulges on the electrode surface. Meanwhile, due to the enormous stress of volume expansion, the internal structure of the electrode gradually changes. Due to the stress, the particles gradually form a powder and fall off in the form of a fluffy morphology (Fig. 9b) that results in poor cycling performance. In Fig. 10b, it can be observed that $SnSbAg_{0.1}$/6% CNT particles distributed evenly in the network, and the whole surface structure changed very little after 10 cycles. During the Li intercalation process, the large diameter of the CNTs provided a large volume of space that was evenly dispersed in the alloy particles, prevented aggregation and increased the buffer space between the alloy particles, which greatly reduced the diffusion distance of the lithium ions and the occurrence of lithium trapping in the active electrode materials. The CNT have excellent mechanical properties and toughness, effectively buffer the enormous stress in the volume expansion of the alloy particles, weakening the forces between the particles and reducing the rate of powder particles. The length (15 um) of the CNTs makes it possible for the CNTs to form the network structure that firmly binds the alloy particles and greatly reduces the shedding of particles, resulting in the good stability of the cycling performance.

4. Conclusions

(1) SnSb–Ag/CNT composite materials were synthesised using chemical reduction methods described in this paper. During the Li intercalation process, CNTs, with a large space volume and formed a network structure, prevented particle aggregation and increased the buffer space between the alloy particles, which greatly reduced the diffusion distance of lithium ions and the occurrence of lithium trapping in the active electrode materials. CNTs also have excellent mechanical properties and toughness, they effectively buffer enormous stresses during the volume expansion of alloy particles, weakening the forces between the particles and reducing the rate of formation of powder particles, resulting in good electrochemical performance.

(2) Silver was used to promote the entire charge–discharge process in the complex multi-step reaction process and, to some extent, alleviate the reunion of the nanoparticles in the reaction process, fully promote the reaction and improve the cycling performance.

(3) $SnSbAg_{0.1}$/6% CNT composite anode exhibited the best cycle performance. The reversible capacity for the 50th cycle was 586.1 mAh g^{-1} between 0.1 and 1.5 V. This anode also maintained good cycling performance at low temperatures.

(4) The $SnSbAg_{0.1}$/6% CNT composite anode exhibited excellent cycle life by controlling the lithiation of the anode material. The reversible capacity for the 50th cycle was 639.6 mAh g^{-1} between 0.05 and 1.5 V.

Acknowledgements

This work was financially supported by Shenzhen Government's Plan of Science and Technology (grant #JCYJ20120613173950029).

References

[1] W.H. Pu, J.G. Ren, C.R. Wan, Z.M. Du, J. Inorg. Mater. 19 (2004) 86–92.
[2] J. Hassoun, A. Fernicola, M.A. Navarra, S. Panero, B. Scrosati, J. Power Sources 195 (2010) 574–579.
[3] C.F. Li, W.H. Ho, C.S. Jiang, C.C. Lai, M.J. Wang, S.K. Yen, J. Power Sources 196 (2011) 768–775.
[4] C. Yin, H. Zhao, H. Guo, W. Qiu, X. Jia, Rare Metal Mater. Eng. 36 (2007) 1403–1406.
[5] H. Zhao, C. Yin, H. Guo, J. He, W. Qiu, Y. Li, J. Power Sources 174 (2007) 916–920.
[6] X.Y. Fan, F.S. Ke, G.Z. Wei, L. Huang, S.G. Sun, Electrochem. Solid State Lett. 11 (2008) A195–A197.
[7] J. Hassoun, G.A. Elia, S. Panero, B. Scrosati, J. Power Sources 196 (2011) 7767–7770.
[8] J. Yang, M. Winter, J.O. Besenhard, Solid State Ionics 90 (1996) 281–287.
[9] N. Pereira, L.C. Klein, G.G. Amatucci, Solid State Ionics 167 (2004) 29–40.
[10] H. Mukaibo, T. Osaka, P. Reale, S. Panero, B. Scrosati, M. Wachtler, J. Power Sources 132 (2004) 225–228.
[11] Z. Wang, W. Tian, X. Li, J. Alloy Compd. 439 (2007) 350–354.
[12] L. Lu, X. Chen, X. Huang, K. Lu, Science 323 (2009) 607–610.
[13] Y. Wang, P. Zhang, X. Ren, G. Yi, J. Electrochem. Soc. 158 (2011) A1404–A1410.
[14] C.M. Park, K.J. Jeon, Chem. Commun. (Camb) 47 (2011) 2122–2124.
[15] J. Hassoun, G. Derrien, S. Panero, B. Scrosati, Electrochim. Acta 54 (2009) 4441–4444.
[16] L.H. Shi, H. Li, Z.X. Wang, X.J. Huang, L.Q. Chen, J. Mater. Chem. 11 (2001) 1502–1505.
[17] H. Li, Q. Wang, L.H. Shi, L.Q. Chen, X.J. Huang, Chem. Mater. 14 (2002) 103–108.
[18] J.N. Coleman, U. Khan, W.J. Blau, Y.K. Gun'ko, Carbon 44 (2006) 1624–1652.
[19] S.Y. Chew, S.H. Ng, J.Z. Wang, P. Novak, F. Krumeich, S.L. Chou, J. Chen, H.K. Liu, Carbon 47 (2009) 2976–2983.
[20] Y. Wang, J.Y. Lee, Angew. Chem. Int. Ed. 45 (2006) 7039–7042.
[21] M.S. Park, S.A. Needham, G.X. Wang, Y.M. Kang, J.S. Park, S.X. Dou, H.K. Liu, Chem. Mater. 19 (2007) 2406–2410.

[22] G.D. Du, C. Zhong, P. Zhang, Z.P. Guo, Z.X. Chen, H.K. Liu, Electrochim. Acta 55 (2010) 2582–2586.
[23] Y. Liu, H. Zheng, X.H. Liu, S. Huang, T. Zhu, J.W. Wang, A. Kushima, N.S. Hudak, X. Huang, S.L. Zhang, S.X. Mao, X.F. Qian, J. Li, J.Y. Huang, Acs Nano 5 (2011) 7245–7253.
[24] Y.R. Jhan, J.G. Duh, S.Y. Tsai, Diam. Relat. Mater. 20 (2011) 413–417.
[25] H. Li, L. Shi, Q. Wang, L. Chen, X. Huang, Solid State Ionics 148 (2002) 247–258.
[26] M.N. Obrovac, L.J. Krause, J. Electrochem. Soc. 154 (2007) A103–A108.
[27] C.M. Park, S. Yoon, S.I. Lee, J.H. Kim, J.H. Jung, H.J. Sohn, J. Electrochem. Soc. 154 (2007) A917–A920.
[28] J.T. Yin, M. Wada, S. Tanase, T. Sakai, J. Electrochem Soc. 151 (2004) A867–A872.